robotics

MDPI

Article

Trajectory Shaping to Reproduce Rod Tip Vibration Suppression in the Rebound Phenomenon of Fly-Casting

Ryosuke Hakamata *, Mitsuru Endo and Yusuke Sugahara

Department of Mechanical Engineering, Institute of Science Tokyo, 2-12-1 Ookayama, Meguro-ku, Tokyo 152-8552, Japan; sugahara.y.ab@m.titech.ac.jp (Y.S.)
* Correspondence: hakamata.r.aa@m.titech.ac.jp; Tel.: +81-80-6747-3920

Abstract

Fly-casting is a throwing technique in which a flexible rod is used to cast a lightweight line. In skilled fly-casting, a phenomenon known as the rebound phenomenon is observed, where the residual vibration of the rod tip is suppressed by the re-acceleration of the rod handle during the rod-stop phase. This vibration suppression plays an essential role in the casting performance; however, an engineering method for this phenomenon has not been established. Therefore, the purpose of this study is to propose a trajectory-shaping method by interpreting the rebound phenomenon as a vibration suppression control problem for flexible systems with nonzero initial conditions. The proposed method applies a conventional shaping framework to rod systems by introducing a second-order approximation and repeatedly shaping the input trajectory to suppress the approximation errors. Through simulations using a rod model, it was shown that the shaped trajectory yields the characteristic re-acceleration of the rod-handle angular velocity during the rod-stop phase, consistent with the rebound phenomenon. Through experiments using a robotic prototype, it was confirmed that the rod tip vibration amplitude is suppressed by over 80% in two types of casting. These results are useful for further studies on the engineering realization of fly-casting.

Keywords: casting manipulation; flexible systems; trajectory shaping; vibration suppression

1. Introduction

Extending the effective workspace of robotic manipulators without increasing the actuator power or the system mass remains an important challenge in robotics. As a source of inspiration, we have focused on "fly-casting", a type of fishing, as a manipulation to address this challenge [1,2]. In typical fishing methods using a lure or a sinker, the lure (or sinker) attached to the tip of a flexible line pulls the line outward by its inertia during the casting motion [3]. However, fly-casting utilizes the elasticity of a rod and the mass of the line itself outside the rod tip [4]. One key feature of fly-casting is that even when the target throwing distance is large, the angler can deliver the fly line to a target spot by performing slow, repetitive motions over a longer period [5,6]. In the long term, this study aims to realize a small and low-power manipulator capable of throwing a line based on the principles of fly-casting.

In fly-casting, after forming the line in the air with a "false casting", the line is placed at the target spot by a "delivery cast". In this study, we focus on false casting. The false casting consists of a "forward cast" and a "back cast". The forward cast involves swinging the rod forward to fly the line in front of an angler. Conversely, the back cast involves

Check for updates

Received: 22 January 2026
Revised: 8 February 2026
Accepted: 9 February 2026
Published: 13 February 2026

Copyright: © 2026 by the authors. Licensee MDPI, Basel, Switzerland. This article is an open access article distributed under the terms and conditions of the Creative Commons Attribution (CC BY) license.

flying the line in the opposite direction. False casting is achieved by repeatedly alternating between these casts [7,8].

In these casts, the rod is swung in the sagittal plane to form a "loop" in the line. The loop is the U-shaped form the line takes immediately after each cast, extending beyond the rod tip. Figure 1 shows the loop formed after a forward cast. The loop consists of sections called the "rod leg", "loop nose", and "fly leg". The rod leg is the lower section connected to the rod tip. The loop nose connects to the rod leg and is the curved front section of the line that flies out by inertia after the cast. The fly leg connects the loop nose to the fly. After the cast, the loop nose flies in the casting direction, resulting in a longer rod leg and shorter fly leg.

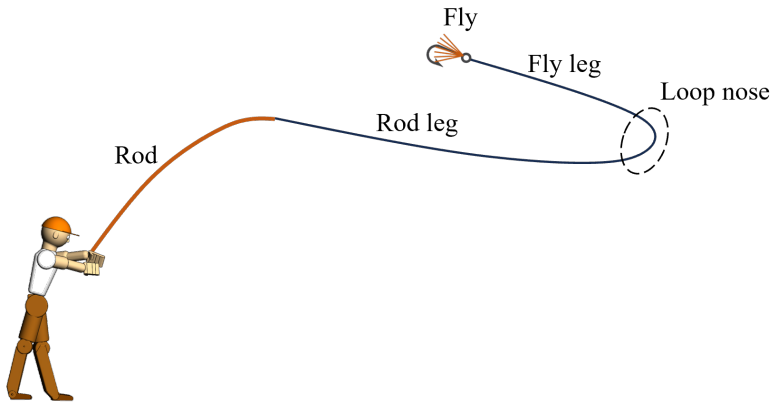


Figure 1. Image of the loop after a forward cast.

This casting is a delicate motion that requires the skill of experts. In this casting process, it is considered important to prevent line slack [9]. Specialists utilize the "rebound phenomenon" as one method to achieve this [10]. Figure 2 illustrates the rebound phenomenon in a forward cast. Here, the rod straight position (RSP) is defined as the instant at which the elastic rod becomes momentarily straight during the casting motion. The rebound phenomenon occurs when, after the RSP at the end of each cast, the rod's inertia causes the rod handle to rotate in the casting direction. Specifically, after the angular velocity of the rod handle decelerates, it accelerates again. The rebound phenomenon is characterized by the suppression of residual vibrations at the rod tip by the re-acceleration of the rod handle after the RSP. This behavior arises from the rod's elastic restoring force and inertia [11]. It has been experimentally demonstrated that this rebound phenomenon suppresses the residual rod vibration [11].

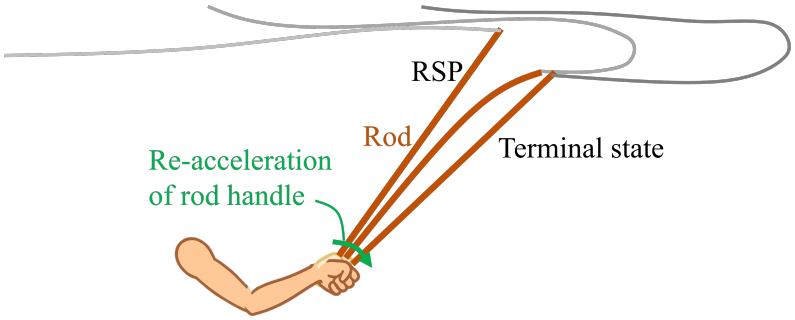


Figure 2. Illustration of the rebound phenomenon in a forward cast. The brown line represents the rod. The motion of the line resulting from following the rod tip movement is shown as a trajectory whose color gradually changes from light to dark, indicating the temporal evolution. The residual vibration at the rod tip is suppressed during the transition from the rod straight position (RSP) to the terminal state, driven by the re-acceleration of the rod handle.

The shape of the rod leg relies on the trajectory of the rod tip from the RSP to the terminal state of the cast. Therefore, the damping effect from this rebound phenomenon is essential for achieving false casting. This rebound phenomenon is one of the skilled techniques for fly-casting experts, based on intuitive operational feel. Therefore, the engineering methodology for achieving the rebound phenomenon remains unclear.

On the other hand, there are several examples of studies that have taken an engineering approach to fly-casting. Several dynamic simulation methods for fly-casting have been proposed. For example, Perkins et al. developed distributed-parameter models of fly-casting by coupling the rod with the line. Their simulations successfully reproduced the loop formation, showing how the elastic energy stored in the rod is transferred to the line [12,13]. Watanabe's method modeled the rod and line as a serial chain composed of multiple links based on multibody dynamics, and numerical simulations were performed [14]. This approach successfully simulated various real-world fly-casting motions [3,4,7,15]. Additionally, Watanabe et al. analyzed the impact of the "rebound phenomenon" on casting [11]. Through simulation and actual equipment verification, they revealed that a slight wrist movement caused by the rebound phenomenon suppresses the residual vibration of the rod after casting. Furthermore, the authors proposed an extension of this method to identify the parameters of the rod model based on its actual behavior [1]. These achievements have made it possible to simulate the actual behavior of fly-casting using numerical computation.

Although various dynamic simulation methods have been proposed, experimental validations with robotic implementations have been limited. The authors developed a robotic system capable of reproducing the false casting motion through a lightweight 3-DOF planar arm equipped with a rod [2]. While this system successfully maintained the line aloft, the joint trajectories were set from real human motions. Therefore, how to swing the rod for a stable false casting remains unclear.

In this study, for the engineering realization of fly-casting, we hypothesize that this phenomenon can be interpreted as a vibration suppression control problem using trajectory shaping for a flexible object, and this hypothesis is verified.

Typical trajectory shaping methods consist of a finite number of delay impulses, and by appropriately setting the weights and delay times, they eliminate the residual vibration for vibration modes. Zero Vibration (ZV) shapers, their extension Zero Vibration Derivative (ZVD) shapers, and the Extra-Insensitive (EI) shaper are the most representative design methods, capable of achieving vibration suppression for single or multiple modes [16,17]. These target trajectories between two static states. However, since the trajectory prior to the RSP affects the shape of the fly leg, it is undesirable to shape it.

On the other hand, Newman et al. proposed an input shaping design for systems with nonzero initial conditions to address this issue [18]. This design method imposes constraints on the shaper to reduce the sensitivity of residual vibrations over a specific frequency range, thereby minimizing the vibrations excited by finite-time disturbances or nonzero initial conditions. Its effectiveness has been demonstrated through simulations and experiments, particularly in research on load sway suppression during crane operations [18].

The problem formulation in this study—suppressing residual vibrations occurring immediately after the RSP through trajectory shaping—is analogous to conventional vibration suppression control problems with nonzero initial conditions. However, unlike existing studies such as crane load sway suppression, this study targets elastic rod systems with multiple vibration modes and preserves the motion before the RSP that determines the fly-leg formation. Accordingly, this study formulates the rebound phenomenon in fly-casting as a vibration suppression problem with nonzero conditions at the RSP.

The purpose of this study is to reproduce the rebound phenomenon in fly-casting based on this formulation and to evaluate its effectiveness through numerical simulations and actual equipment verification.

2. Problem Statement

Although fly-casting inherently involves the dynamics of the fly line, this study intentionally focuses on reproducing the rebound phenomenon through rod motion alone. The purpose of this simplification is to isolate the fundamental mechanics of the rebound phenomenon associated with the elastic rod and to examine whether the characteristic vibration behavior after the RSP can be reproduced without explicitly modeling the line dynamics.

This study considers the motion of a planar three-degrees-of-freedom (3-DOF) arm with an elastic rod attached at the end for a forward cast. Performing trajectory shaping to accumulate and release the rod's elastic energy for line acceleration degrades the casting performance. Therefore, this study defines a vibration suppression control problem in a nonzero state: detecting the instant when the rod is in the RSP and shaping the trajectory only for the brief period from that point to the end. Here, let t_s denote the timing of the RSP, and let t_{end} denote the timing of the terminal state. Denoting the time interval to be shaped as T, t_{end} can be expressed as $t_s + T$.

The arm's initial joint trajectory $[\theta_s(t), \theta_e(t), \theta_w(t)]\, t \in [0\, t_s + T]$ is generated by interpolating the starting and ending angles of the actual false casting arm using the following Gaussian function, as in the previous study [4]:

$$\dot{\theta}_i(t) = \frac{\theta_{i,\mathrm{scale}}}{\sqrt{2\pi}\sigma_i} \exp\left(-\frac{(t-\mu_i)}{2\sigma_i^2}\right), \quad i \in [s, e, w], \tag{1}$$

where $\theta_{i,\mathrm{scale}}$ represents the rotational angle of each link in the initial trajectory. The initial angle $[\theta_s(0), \theta_e(0), \theta_w(0)]$ and rotation angle $[\theta_{s,\mathrm{scale}}, \theta_{e,\mathrm{scale}}, \theta_{w,\mathrm{scale}}]$ are set by referencing the behavior of human casts measured in the previous study [4]. In this formulation, the Gaussian function is used as a deterministic shape function to generate a smooth joint velocity profile.

By detecting the rod straight position (RSP) along this trajectory, the system state at the RSP timing t_s is regarded as a new initial condition. Subsequently, trajectory shaping is applied only in the interval $[t_s,\ t_s + T]$ to suppress the rod vibration.

The effects of the line attached to the rod tip are outside the scope of this study and will be discussed in a future paper. This evaluation focuses on how much vibration is suppressed based on the trajectory of the rod tip.

3. Dynamic Model of an Elastic Rod

The full dynamic model of the elastic rod is presented in this section. The modeling framework follows the method developed by Watanabe et al. [14], who successfully applied it to a variety of fly-casting analyses. This section provides a brief overview of the model and the notations used in this article; the derivation and implementation details are given in our previous work [1].

The rod is modeled as a planar chain composed of multiple rigid links connected by rotational joints, each connected with rotational springs and dampers, as shown in Figures 3 and 4. A planar 3-DOF arm (shoulder, elbow, and wrist) is connected to the base link of the elastic rod.

For the i-th link, its center of mass is denoted by $\mathrm{G}_i(x_i, y_i)$, and the rotational joint connecting the i-th and $(i+1)$-th links is denoted by J_i. The mass of the i-th link is m_i, its

moment of inertia is I_i, the distance from G_i to J_i is l_{iR}, and the distance from J_i to G_i is l_{iL}. The spring constant and damping coefficient of J_i are k_i and c_i, respectively.

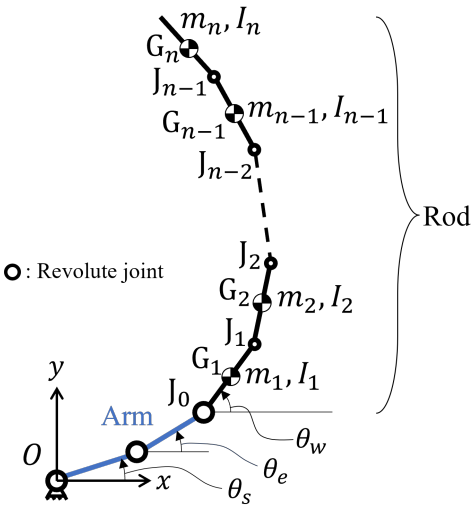


Figure 3. Dynamic modeling of rod and arm. The black-and-white checkered circles indicate the center of mass of each link.

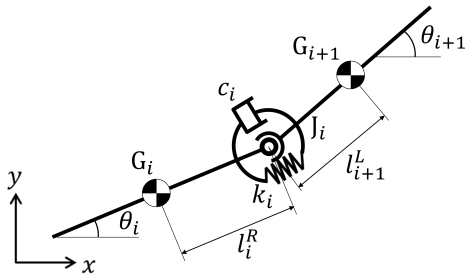


Figure 4. Joint with rotational spring and damper. The black-and-white checkered circles indicate the center of mass of each link.

The generalized coordinates $\boldsymbol{r} \in \mathbb{R}^{2n}$ and $\boldsymbol{\phi} \in \mathbb{R}^n$, as well as the generalized force $\boldsymbol{Q} \in \mathbb{R}^{3n}$, are defined as follows:

$$\begin{aligned} \boldsymbol{r} &= [x_1, y_1, \ldots, x_n, y_n], \\ \boldsymbol{\phi} &= [\theta_1, \theta_2, \ldots, \theta_n], \\ \boldsymbol{Q} &= [\boldsymbol{Q}_r^T, \boldsymbol{Q}_\phi^T]^T, \end{aligned}$$

where θ_i denotes the rotation angle of the i-th link defined with respect to the global coordinate frame. Assuming no air drag, $\boldsymbol{Q}_r \in \mathbb{R}^{2n}$ represents the gravitational vector, and $\boldsymbol{Q}_\phi \in \mathbb{R}^n$ represents the generalized joint torque, which consists of passive torques from springs and dampers and active torques $\tau_{\text{base}} \in \mathbb{R}$ applied at J_0.

Watanabe et al. modeled the rod for various fly-casting simulations using the Lagrange multiplier method [14] as follows:

$$\begin{bmatrix} M_r & O_{2n\times n} & \boldsymbol{\Phi}_{\boldsymbol{r}}^T \\ O_{n\times 2n} & M_\phi & \boldsymbol{\Phi}_{\boldsymbol{\phi}}^T \\ \boldsymbol{\Phi}_{\boldsymbol{r}} & \boldsymbol{\Phi}_{\boldsymbol{\phi}} & O_{2n\times 2n} \end{bmatrix} \begin{bmatrix} \ddot{\boldsymbol{r}} \\ \ddot{\boldsymbol{\phi}} \\ \boldsymbol{\lambda} \end{bmatrix} = \begin{bmatrix} \boldsymbol{Q}_r \\ \boldsymbol{Q}_\phi \\ \boldsymbol{\gamma} \end{bmatrix}, \tag{2}$$

where $\boldsymbol{\lambda} \in \mathbb{R}^{2n}$ is the Lagrange multiplier vector, $M_r \in \mathbb{R}^{2n\times 2n}$ is the mass matrix, and $M_\phi \in \mathbb{R}^{n\times n}$ is the inertia tensor. $\boldsymbol{\Phi}_r$ and $\boldsymbol{\Phi}_{\boldsymbol{\phi}}$ represent the partial derivatives of

constraints $\boldsymbol{\Phi} \in \mathbb{R}^{2n}$ with respect to $\boldsymbol{r}$ and $\boldsymbol{\phi}$, respectively. Here, $\boldsymbol{\Phi}$ represents the constraints derived from the geometric relationships of the links.

The constraints $\boldsymbol{\Phi}$ are expressed as follows based on the geometric relationships of the links:

$$\boldsymbol{\Phi}_i = \begin{bmatrix} x_{i-1} + l_R^i \cos\theta_{i-1} + l_L^i \cos\theta_i - x_i \\ y_{i-1} + l_R^i \sin\theta_{i-1} + l_L^i \sin\theta_i - y_i \end{bmatrix}, \tag{3}$$

$$\boldsymbol{\Phi} = \begin{bmatrix} \boldsymbol{\Phi}_1^T & \boldsymbol{\Phi}_2^T & \cdots & \boldsymbol{\Phi}_n^T \end{bmatrix}^T = \mathbf{0}, \tag{4}$$

where (x_0, y_0) represents the origin of the planar coordinates.

The vector $\boldsymbol{\gamma} \in \mathbb{R}^{2n}$ is derived as follows:

$$\boldsymbol{\gamma} = -\frac{\partial}{\partial \boldsymbol{\phi}} \left(\frac{\partial \boldsymbol{\Phi}}{\partial \boldsymbol{\phi}} \dot{\boldsymbol{\phi}} \right) \dot{\boldsymbol{\phi}}. \tag{5}$$

The equation of motion with respect to $\boldsymbol{\phi}$ is derived as follows:

$$\ddot{\boldsymbol{\phi}} = (M^*)^{-1} \boldsymbol{Q}^*. \tag{6}$$

M^* and $\boldsymbol{Q}^*$ are defined as follows:

$$M^* = M_\phi + \boldsymbol{\Phi}_\phi^T (\boldsymbol{\Phi}_{\boldsymbol{r}}^T)^{-1} M_r \boldsymbol{\Phi}_r^{-1} \boldsymbol{\Phi}_{\boldsymbol{\phi}}, \tag{7}$$

$$\boldsymbol{Q}^* = \boldsymbol{Q}_\phi - \boldsymbol{\Phi}_{\boldsymbol{\phi}}^T (\boldsymbol{\Phi}_{\boldsymbol{r}}^T)^{-1} (\boldsymbol{Q}_r - M_r \boldsymbol{\Phi}_{\boldsymbol{r}}^{-1} \boldsymbol{\gamma}). \tag{8}$$

Using this model, the behavior of the rod can be obtained relative to the behavior of the rod base link.

4. Trajectory Shaping Method Based on the Reconstruction of Rod Model

In this section, we propose a trajectory shaping method to suppress residual vibrations at the rod tip after the RSP. This is achieved by modeling the motion as a second-order system and shaping the terminal state to zero. This shaping is realized by applying a smooth correction to the wrist acceleration during the period immediately following the RSP until the rod comes to a stop.

4.1. Overview of Method

A flowchart of the proposed trajectory shaping method is shown in Figure 5.

At the RSP, the wrist, the first section of the rod, and the rod tip align almost in a straight line, and the elastic energy stored in the rod is almost completely released. After this RSP, the wrist is moved to rapidly decelerate and stop the rod base. In our previous measurements of the rod free vibration [1], the rod tip response was predominantly governed by the first vibration mode. Since the wrist is rapidly decelerated after the RSP, the rod motion is expected to be similar to a free-vibration response, and a similar dominance of the first mode is expected.

In this study, parameters related to the vibration motion (natural frequency and damping ratio) are estimated from the trajectory of the rod tip obtained during this period. This estimation allows the motion of the rod tip to be represented as a second-order system model, enabling the application of the conventional trajectory shaping method.

For the second-order model, the correction trajectory for the wrist joint angular acceleration is determined such that the displacement and velocity at the termination point are zero. Here, the correction trajectory is obtained as the minimum-norm solution in a

smooth function space. This suppresses residual vibration while avoiding pulse inputs and discontinuous angular acceleration changes.

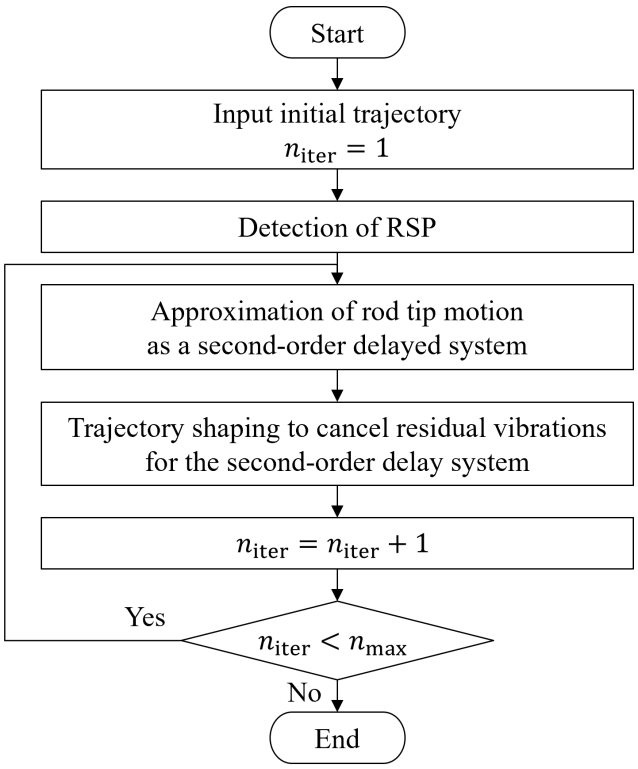


Figure 5. Flowchart for trajectory shaping.

Finally, the obtained correction trajectory is added to the wrist joint angular acceleration to reconstruct the wrist joint angular trajectory. Previous studies focused on second-order systems, where residual vibrations were nearly eliminated by the optimized correction trajectory. In contrast, this study addresses systems with higher-order vibration modes, where approximation errors cause residual vibrations to persist. Therefore, this study suppresses the residual vibrations caused by approximation errors by applying multiple input shaping.

4.2. Second-Order System Based on Rod Tip Motion

In this section, the vibration of the rod tip during the time interval $I = [t_s,\ t_s + T]$ after the correction start time t_s is approximated as a second-order system.

Let the displacement of the rod tip from the RSP observed in the correction section be denoted as $y_\perp(t)$. Introduce a second-order system $\delta(t)$, and approximate $y_\perp(t)$ as follows:

$$y_\perp(t) \approx L_2\,\delta(t), \tag{9}$$

where $L_2 > 0$ denotes a positive link length. $\delta(t)$ is defined as follows:

$$\ddot{\delta}(t) + 2\zeta\omega_n\dot{\delta}(t) + \omega_n^2\,\delta(t) = -\gamma_{\text{in}}\,u(t), \tag{10}$$

where $\omega_n > 0$ is the natural frequency, $\zeta \in [0, 1)$ is the damping ratio, $-\gamma_{\text{in}}$ is the input gain, and $u(t) = \ddot{\theta}_w(t)$ is the wrist angular acceleration. γ_{in} is a parameter set by the designer.

From the waveform of $y_\perp(t)$, determine L_2 and the damped natural frequency $\omega_d = \omega_n\sqrt{1-\zeta^2}$, and from the amplitude damping, determine ζ.

4.3. Input Shaping Method for a System with Nonzero Initial Conditions

This section explains the input shaping method based on the reference [18].

Here, (10) can be expressed as follows:

$$\dot{\boldsymbol{x}}(t) = A\,\boldsymbol{x}(t) + B\,u(t), \qquad A = \begin{bmatrix} 0 & 1 \\ -\omega_n^2 & -2\zeta\omega_n \end{bmatrix}, \quad B = \begin{bmatrix} 0 \\ -\gamma_{\text{in}} \end{bmatrix}, \quad \boldsymbol{x}(t) = \begin{bmatrix} \delta(t) \\ \dot{\delta}(t). \end{bmatrix}. \tag{11}$$

For the period $[0, T]$ (where $t = t_s$ is the origin), the state at $t = T$ can be derived as follows:

$$\boldsymbol{x}(T) \;=\; e^{AT}\boldsymbol{x}(0) + \int_0^T e^{A(T-\tau)} B\,u(\tau)\,d\tau. \tag{12}$$

For the input trajectory u_{nom} before shaping, its residual can be expressed as follows:

$$x_b = e^{AT}\boldsymbol{x}(0) + \int_0^T e^{A(T-\tau)} B\,u_{\text{nom}}(\tau)\,d\tau. \tag{13}$$

The correction u_{corr} that zeroes the terminal state by overlaying satisfies the following equation:

$$\int_0^T e^{A(T-\tau)} B\,u_{\text{corr}}(\tau)\,d\tau \;=\; -\,x_b = -[X_b\ V_b]^\top. \tag{14}$$

The damped natural frequency $\omega_d = \omega_n\sqrt{1-\zeta^2}$, introducing the exponent $\alpha = \zeta\omega_n$, allows $e^{A(T-\tau)}B$ to be expressed as the sum of two scalar kernels $g(\tau)$ and $h(\tau)$ as follows:

$$\int_0^T g(\tau)\,u_{\text{corr}}(\tau)\,d\tau \;=\; -X_b, \qquad \int_0^T h(\tau)\,u_{\text{corr}}(\tau)\,d\tau \;=\; -V_b, \tag{15}$$

$$g(\tau) = -\,\gamma_{\text{in}}\,e^{-\alpha(T-\tau)}\,\frac{1}{\omega_d}\,\sin(\omega_d(T-\tau)), \tag{16}$$

$$h(\tau) = -\,\gamma_{\text{in}}\,e^{-\alpha(T-\tau)}\left[\cos(\omega_d(T-\tau)) - \frac{\alpha}{\omega_d}\,\sin(\omega_d(T-\tau))\right]. \tag{17}$$

Here, (15) is a linear weighted constraint on u_{corr}, and if (A, B) is controllable, a correction trajectory must exist.

4.4. Computation of Smooth Correction Trajectory Using Bernstein Basis Polynomials

For a smooth correction trajectory, the interval $[0, T]$ is non-dimensionalized as $s = t/T \in [0,1]$, and $u_{\text{corr}}(t)$ is represented by a smooth basis C^1 and vanishes at both endpoints:

$$u_{\text{corr}}(t) \;=\; \sum_{i=0}^{m} a_i\,\phi_i\!\left(\frac{t}{T}\right), \qquad \phi_i(s) \;=\; s(1-s)\,B_i^{(m)}(s), \tag{18}$$

where $B_i^{(m)}(s) = \binom{m}{i}s^i(1-s)^{m-i}$ is the Bernstein polynomial. This is inspired by the smooth distributed-delay shaping method proposed by Singh et al. [19]. Since $\phi_i(0) = \phi_i(1) = 0$, the velocity discontinuity at the boundary of the orbit is avoided. Consequently, (15) can be expressed as follows for the basis coefficients $\boldsymbol{a} \in \mathbb{R}^{m+1}$:

$$\sum_{i=0}^{m} a_i \underbrace{\int_0^T g(\tau)\,\phi_i\!\left(\tfrac{\tau}{T}\right)d\tau}_{:=M_{x,i}} = -X_b, \qquad \sum_{i=0}^{m} a_i \underbrace{\int_0^T h(\tau)\,\phi_i\!\left(\tfrac{\tau}{T}\right)d\tau}_{:=M_{v,i}} = -V_b. \tag{19}$$

From the above, the following linear equality constraints can be derived.

$$\underbrace{\begin{bmatrix} M_x \\ M_v \end{bmatrix}}_{C \in \mathbb{R}^{2\times(m+1)}} a \;=\; -\underbrace{\begin{bmatrix} X_b \\ V_b \end{bmatrix}}_{d \in \mathbb{R}^2}. \tag{20}$$

Due to the definitions of $g(\tau)$ and $h(\tau)$, since the two rows of C are linearly independent, the solution set exists if $m+1 \geq 2$, and the minimum-norm solution can be computed using pseudo inverse computation.

4.5. Minimum-Norm Solution Subject to Constraints and Discrete Implementation on Discrete Time System

To handle the continuous-time correction input $u_{\mathrm{corr}}(t)$ in numerical optimization, the interval $[0, T]$ is discretized as $t_k = kh$ $(k = 0, \ldots, N-1)$ and sampled. Let $\Phi \in \mathbb{R}^{N\times(m+1)}$ be defined by $\Phi_{k,i} = \phi_i(k/(N-1))$, and define the family of correction trajectories as $u = \Phi a$. Here, the following objective function is defined:

$$J(a) \;=\; \lambda_0 \|u\|_2^2 + \lambda_1 \|D_1 u\|_2^2 + \lambda_2 \|D_2 u\|_2^2, \tag{21}$$

where D_1 and D_2 are the first-order and second-order difference matrices, respectively, and $\lambda_i \geq 0$ is a weight coefficient, which is a parameter determined by the designer. In the proposed formulation, the suppression of rod tip vibration is imposed as a constraint through the second-order model approximation, under which the residual vibration can be ideally eliminated. The input u is minimized to select the least intrusive correction that preserves the original arm motion as much as possible.

Then, (21) can be expressed as follows:

$$J(a) \;=\; a^\top Q\, a, \qquad Q \;=\; \lambda_0 \Phi^\top \Phi + \lambda_1 (D_1\Phi)^\top (D_1\Phi) + \lambda_2 (D_2\Phi)^\top (D_2\Phi). \tag{22}$$

Here, (20) can be expressed numerically as follows:

$$Ca = -d, \qquad C := \begin{bmatrix} \mathbf{1}^\top W\, G\, \Phi \\ \mathbf{1}^\top W\, H\, \Phi \end{bmatrix}, \quad d := \begin{bmatrix} X_b \\ V_b \end{bmatrix}, \tag{23}$$

$$G = \begin{bmatrix} g(\tau_0) \\ \vdots \\ g(\tau_{N-1}) \end{bmatrix}, \qquad H = \begin{bmatrix} h(\tau_0) \\ \vdots \\ h(\tau_{N-1}) \end{bmatrix}, \tag{24}$$

where W is the weight matrix for the trapezoidal integral. The optimal solution to this quadratic programming problem is obtained by solving the following KKT conditions derived from the Lagrangian $\mathcal{L}(a, \lambda) = a^\top Q a + \lambda^\top (Ca + d)$.

$$\begin{bmatrix} 2Q & C^\top \\ C & 0 \end{bmatrix} \begin{bmatrix} a \\ \lambda \end{bmatrix} \;=\; \begin{bmatrix} 0 \\ -d \end{bmatrix}. \tag{25}$$

Here, since $Q \succeq 0$, $\mathrm{rank}(C) = 2$, a unique minimal-norm solution is obtained.

The obtained u_{corr} is overlaid to the wrist joint angular acceleration as follows to reconstruct the wrist joint angular trajectory.

$$\ddot{\theta}_{w,\mathrm{new}}(t) \;=\; \ddot{\theta}_w(t) + \beta u_{\mathrm{corr}}(t), \tag{26}$$

where β is a coefficient multiplied by the correction trajectory and is a parameter determined by the designer. When $\beta = 1$, $\boldsymbol{x}(T) = 0$ is achieved at the terminal point, and the residual

vibration of the approximated second-order system is theoretically eliminated. However, since the actual system differs from a second-order system, a trajectory multiplied by the constant β is added to account for the modeling errors.

4.6. Compensation for Modeling Errors via Multiple Shaping

A single shaping achieves complete damping for a second-order system model. However, since actual rods possess multiple modes, residual vibration due to modeling errors is expected to remain by a single approximation as a second-order system.

Therefore, this study proposes a method to progressively suppress the effects of modeling errors by applying shaping multiple times. At each iteration, the vibration modes (natural frequency ω_n and damping ratio ζ) are re-estimated from the shaped motion data, and the shaping is redesigned based on these values. This allows the shaping to be readjusted for each frequency where the second-order approximation holds, thereby suppressing the residual vibrations. Let the number of shaping iterations be denoted by $n_{\max}$.

5. Verification of Shaping Methods Through Simulations

In this section, we evaluate the effectiveness of the trajectory shaping method for a system with nonzero initial conditions, based on the identification of a second-order rod model. Here, the effects of the number of shaping iterations and the shaping parameters on the vibration suppression performance, the amplitude decay, are discussed.

5.1. Simulation Method and Conditions

The simulation employed the dynamic model of the rod identified in our previous study [1]. The parameters used in the simulation are listed in Table 1. The time step was set to $\Delta t = 1$ ms, the casting time was set to $t_{\text{end}} = 0.8$ s, the initial joint angles $[\theta_s(0), \theta_e(0), \theta_w(0)]$ were set to a horizontal configuration, and the initial target displacement $[\theta_{s,\text{scale}}, \theta_{e,\text{scale}}, \theta_{w,\text{scale}}]$ was determined based on the actual lifting motion. The damping effect was evaluated using the peak-to-peak value after the RSP.

Table 1. Simulation parameters.

Parameters	Values
l_i [mm]	$[328, 760, 559, 623, 388]$
l_i^L [mm]	$[116, 370, 270, 285, 210]$
k_i [N·m/rad]	$[24.3, 7.93, 3.23, 0.631]$
c_i [N·m·s/rad]	$[4.91 \times 10^{-2}, 1.60 \times 10^{-2}, 5.43 \times 10^{-3}, 7.31 \times 10^{-4}]$
m_i [g]	$[37.7, 28.8, 12.5, 11.5, 6.52]$
I_i [kg·m^2]	$[32.7, 13.8, 3.23, 3.52, 0.761] \times 10^{-4}$
t_{end}	0.8
$[\mu_s, \mu_e, \mu_w]$	$[0.45, 0.50, 0.60] \times t_{\text{end}}$
$[\lambda_1, \lambda_2, \lambda_3]$	$[10^{-3}, 10^{-4}, 10^{-6}]$
$[\theta_s(0), \theta_e(0), \theta_w(0)]$ [deg]	[0, 0, 0]
$[\theta_{s,\text{scale}}, \theta_{e,\text{scale}}, \theta_{w,\text{scale}}]$ [deg]	[10, 30, 90]
Time step [ms]	1

5.2. Evaluation of Iterative Shaping

In this section, we first examine the validity of the second-order approximation for the rod tip dynamics after RSP and then evaluate the damping performance when varying the number of shaping iterations.

Figure 6 compares the rod tip displacement obtained from the full rod simulation with that predicted by the identified second-order model under the same initial condition at the RSP. The two responses show close agreement in both oscillation frequency and amplitude decay after the RSP, indicating that the rod tip dynamics are reasonably approximated by a second-order system in this phase.

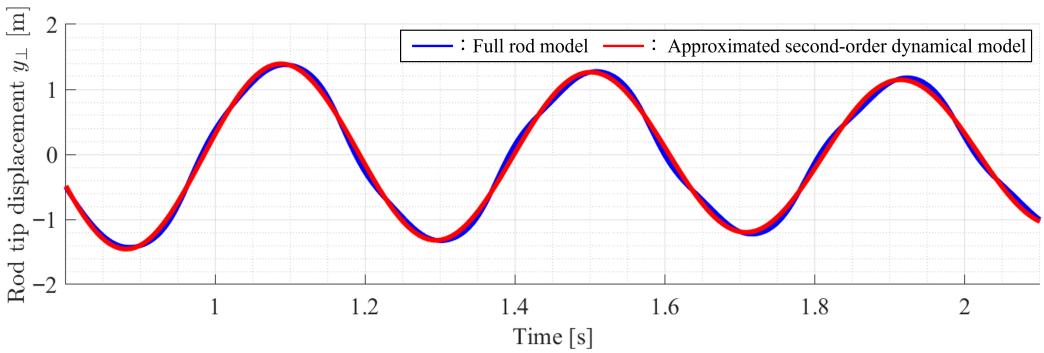


Figure 6. Comparison of the rod tip displacement after the RSP, obtained from the full rod model and the approximated second-order dynamical model. The blue line represents the response of the full rod model, while the red line represents the response of the approximated second-order dynamical model.

Based on this approximation, the damping performance was evaluated by varying the number of shaping iterations. The motion of the rod tip was simulated under six conditions, corresponding to the number of shaping iterations $n_{\max} = 0, 1, \cdots, 5$. Here, $n_{\max} = 0$ corresponds to the baseline motion without shaping, $n_{\max} = 1$ corresponds to a single shaping iteration, and $n_{\max} \geq 2$ corresponds to the iterative shaping in the proposed method.

Table 2 shows the peak-to-peak values of the residual vibration according to each number of shaping iterations. Figure 7 shows the path of the rod tip for each number of shaping iterations. While tip vibration clearly remains in the case of $n_{\max} = 0$ and $n_{\max} = 1$, it is significantly suppressed for $n_{\max} \geq 2$. However, excessively increasing the shaping number to $n_{\max} \geq 3$ does not yield further damping effects. This residual vibration seems to be due to modeling errors, and fully suppressing it remains for future work.

Table 2. Comparison of the peak-to-peak values of the residual vibration according to the number of shaping iterations.

The number of shaping iterations $n_{\max}$	0	1	2	3	4	5
The peak-to-peak values [m]	2.804	1.289	0.785	0.470	0.542	0.629

These results indicate that the number of shaping iterations can be selected through numerical simulations based on the rod model to achieve sufficient vibration suppression.

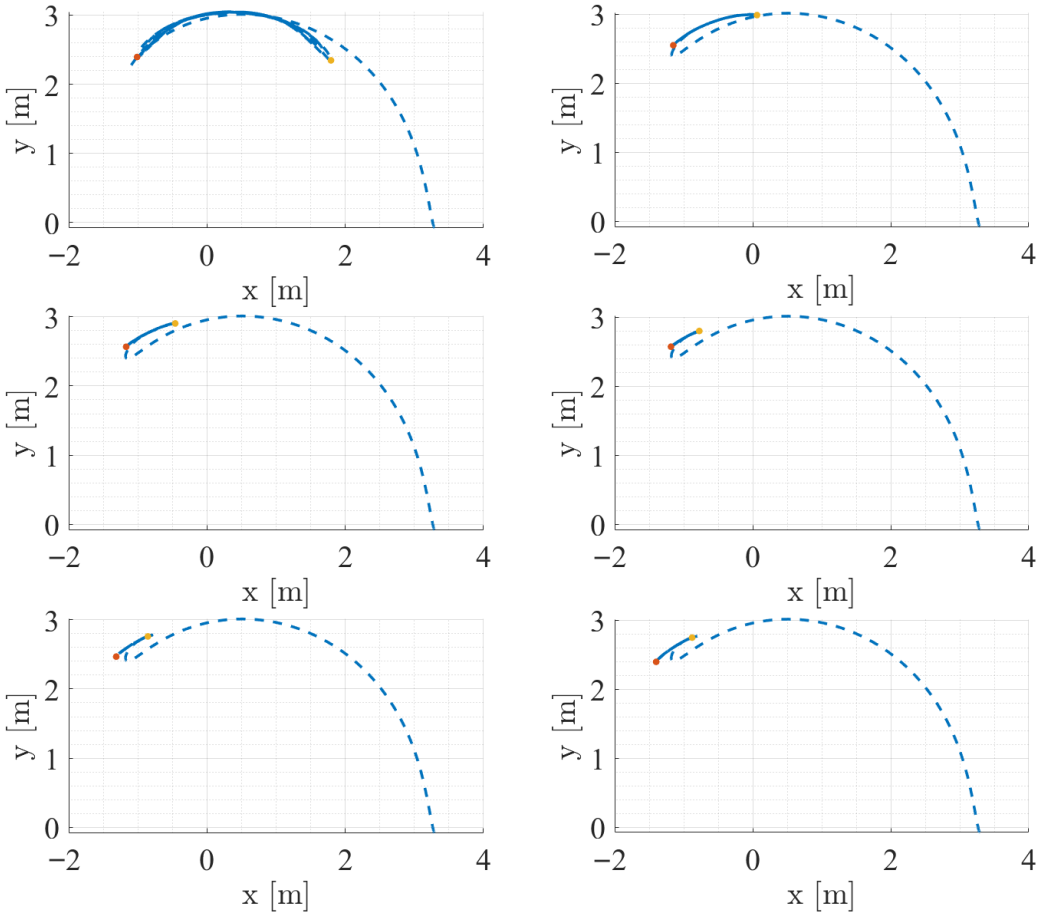


Figure 7. Rod tip trajectories for each number of shaping iterations. The dashed line indicates the path of the rod tip during the upward swing. The solid line indicates the vibrating portion of the rod tip after passing the RSP. The red and yellow dots indicate the two end positions corresponding to the peak-to-peak amplitude of the vibration after the RSP. The residual vibration of the tip decreases as shaping is repeated, and a minimum is observed at $n_{\max} = 3$.

5.3. Parameter Sensitivity Analysis

This section evaluates the effects of the shaping parameters γ_{in}, β, and the target displacement $\theta_{w,\text{scale}}$ on the damping performance in the proposed method.

5.3.1. The Effects of γ_{in} and β

The number of iterations was fixed at three, and the variation in peak-to-peak values for each set of γ_{in} and β is shown in Figure 8. The peak-to-peak value exhibits a convex variation, indicating that the minimum value $(\gamma_{\text{in}}^*, \beta^*)$ can be obtained.

This result clarifies how each shaping parameter affects the vibration suppression performance. Therefore, numerical simulations based on the rod model can confirm the trend of parameter tuning and serve as a guide for determining the values of design parameters.

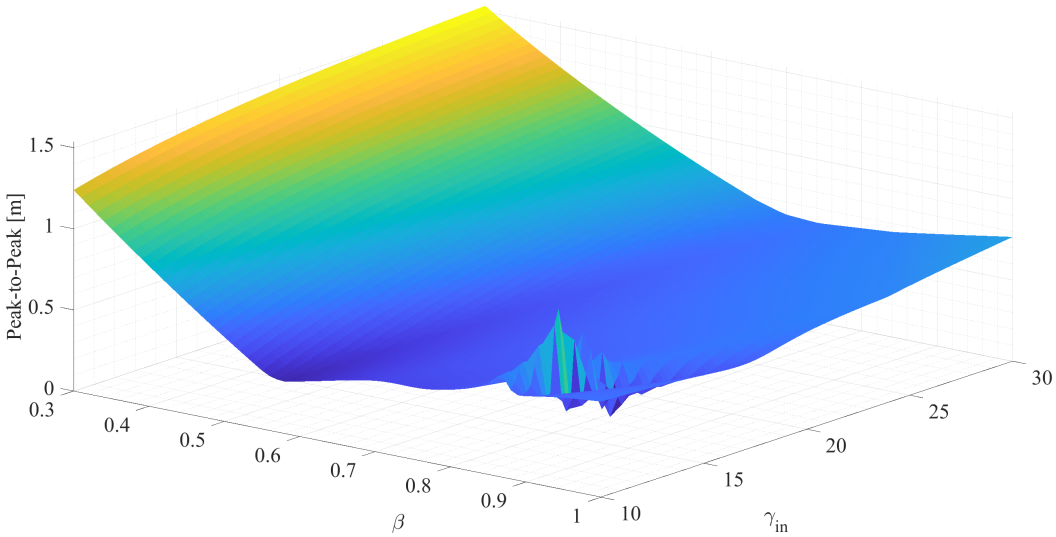


Figure 8. Peak-to-peak values for each pair of γ_{in} and β. The color represents the magnitude of the peak-to-peak vibration amplitude for each combination of γ_{in} and β.

5.3.2. The Effects of the Wrist Joint Displacement $\theta_{w,\text{scale}}$

Next, the effects of the wrist joint displacement $\theta_{w,\text{scale}}$ on the vibration suppression performance were evaluated. The results confirm that the post-shaping terminal angle $\theta_{w,\text{new}}$ varies nearly linearly with $\theta_w(t_{\text{end}})$ (Figure 9). Therefore, if the target terminal angle $\theta_{w,\text{new}}$ is determined, $\theta_w(t_{\text{end}})$ can be approximately determined by inverting this relationship. This property is expected to facilitate setting the initial search range in iterative reshaping.

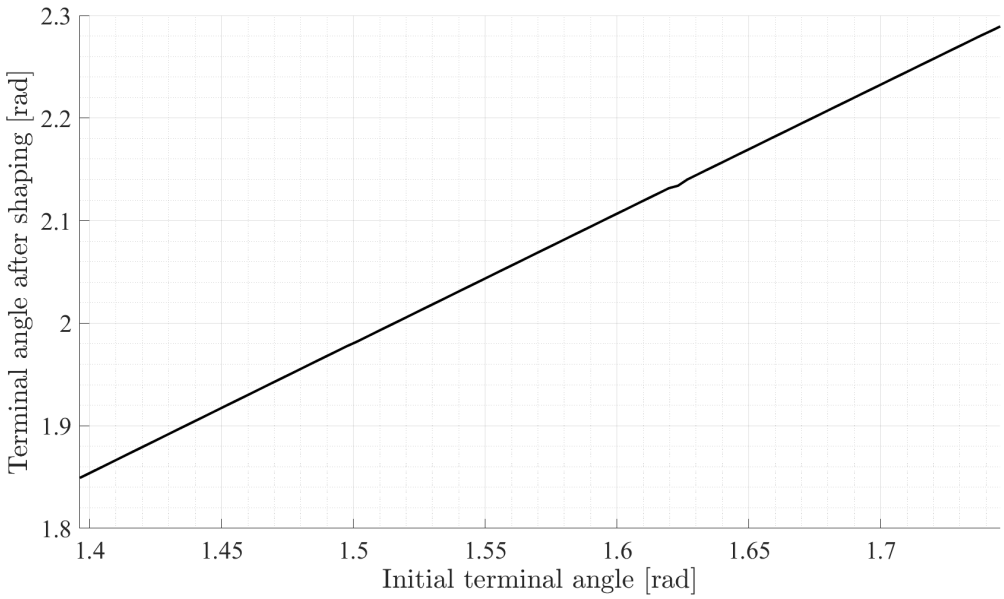


Figure 9. Relationship between the terminal angle θ_{end} and $\theta_{w,\text{new}}$. An approximately linear trend is observed, with a slope of 1.261.

Thus, we confirmed that the main parameters γ_{in}, β, and $\theta_{w,\text{scale}}$ in the proposed method all exert predictable effects on damping performance. In particular, an optimal region exists for combinations of γ_{in} and β, and $\theta_{w,\text{scale}}$ can be used for the approximate estimation of the terminal angle.

5.4. Comparison with the Actual Rebound Phenomenon

Here, we discuss the relationship between the trajectory shaping obtained by the proposed method and the rebound phenomenon in fly-casting.

The angular velocity of the shaped wrist joint is shown in Figure 10, with the number of iterations $n_{\max}$ fixed at three. The rebound phenomenon, in which the rod handle is re-accelerated, is reproduced. Moreover, combined with the results from the previous sections, we showed that the proposed method is effective in reproducing the rebound phenomenon, providing this corrected angular velocity trajectory and suppressing residual vibration at the rod tip. Therefore, the trajectory shaping method can realize the rebound phenomenon.

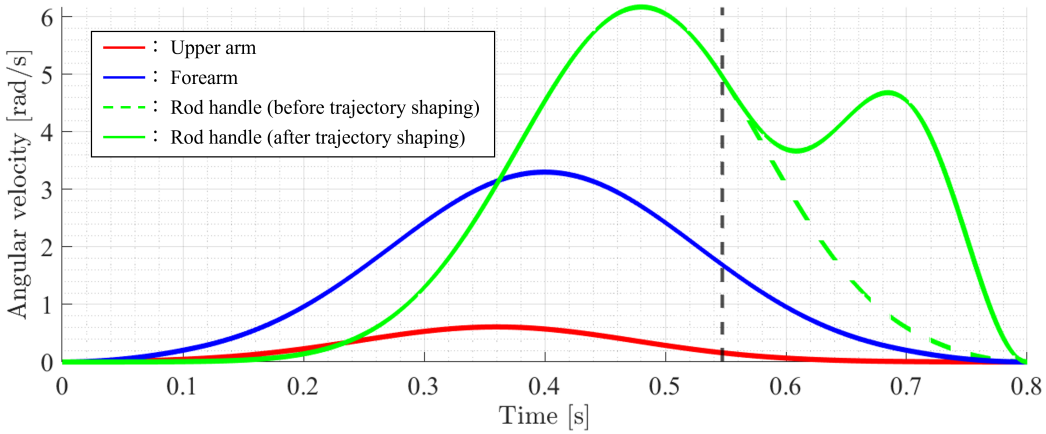


Figure 10. Angular velocity of each link before and after trajectory shaping. The red line represents the rotational angular velocity of the upper arm, the blue line represents the forearm, and the green line represents the rod handle. The green dashed line indicates before trajectory shaping, while the solid line indicates after trajectory shaping. The timing of the RSP is indicated by the black dashed line.

6. Verification of Shaping Methods Through Experiments Using a Prototype

In this section, we describe the experimental validation using a prototype, which showed the effectiveness of the terminal state shaping method for a system with nonzero initial conditions, based on the identification of a second-order rod model Here, both forward cast and back cast in false casting were considered.

6.1. Experimental Conditions

The durations of both the forward cast and back cast were set to $t_{\text{end}} = 0.8$ s. The initial trajectory before shaping was defined, as in the simulations, using a Gaussian function. Here, we set $[\theta_s(0), \theta_e(0), \theta_w(0)] = [-10, 60, 95]$ [deg] and $[\theta_{s,\text{scale}}, \theta_{e,\text{scale}}, \theta_{w,\text{scale}}] = [20, -30, -35]$ [deg]. The experimental prototype (Figure 11) used in this study is the same as that reported in our previous work [2]. Detailed specifications and design of the prototype are therefore omitted here and can be found in [2]. The elastic rod was the DAIWA LOCHMOP F865-4 (97 g), an actual fly-fishing rod used in practice. Motion capture equipment, OptiTrack Flex 13, was used for measurement at 120 Hz. The measurement software was Motive 3.2.0, and the analysis was performed using MATLAB R2023a. According to the manufacturer specifications [20], the positional accuracy of the motion capture system is approximately 0.1 mm. Reflective sheets were attached to the rod, and its motion was recorded using 10 tracking cameras (NaturalPoint, Inc., Corvallis, OR, USA).

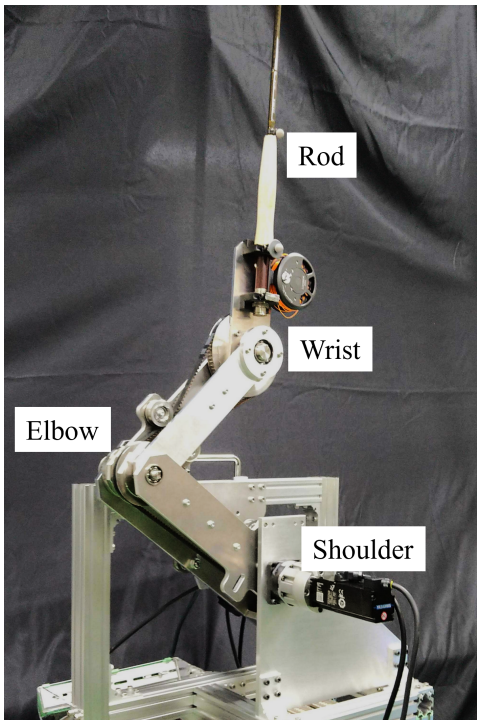


Figure 11. Photo of experimental prototype.

6.2. Experimental Results

The rod motion and rod tip trajectory before applying the proposed method during forward cast and back cast are shown in Figure 12a and 12b, respectively. Similarly, the rod motion and rod tip trajectory after applying the proposed method during forward cast and back cast are shown in Figure 12c and 12d, respectively. In these figures, the rod configurations at the casting start and at both ends of the maximum amplitude are represented by brown curves. The blue curves represent the rod tip trajectories for 2 s after the start of each cast. The two ends of the vibration after the RSP are represented by green points. To visually illustrate the changes in rod tip trajectories, the trajectories of the rod tip's x-coordinate and y-coordinate during the forward cast are shown in Figure 13. The blue line indicates the trajectory before shaping, while the brown line indicates the trajectory after shaping.

From the comparison of the four figures, it can be observed that after applying the proposed method, the bending of the rod in the rod-stop phase is reduced. In the forward cast before vibration suppression, the peak-to-peak value was 1.10 m. After suppression, this was reduced to 0.190 m, corresponding to an amplitude reduction of 82.7%. In the backward cast before suppression, the peak-to-peak value was 1.22 m. After suppression, this was reduced to 0.0768 m, corresponding to a reduction of 93.2%.

Additionally, the forward cast was repeated three times before and after shaping, and the peak-to-peak values for each are shown in Table 3. As shown in this table, the peak-to-peak vibration amplitude is reduced from an average of 1.16 m before shaping to 0.179 m after shaping, corresponding to an approximate reduction of 85%. This substantial reduction was consistently observed across all three trials.

Hence, the proposed method is effective for suppressing residual vibration after casting in false casting.

It should be noted that this study has several limitations. First, the experiments were conducted using a rod-only configuration without an attached line. Although this simplification allows isolation of the rebound phenomenon associated with the elastic rod, the inclusion of line dynamics may alter the quantitative performance of the proposed

trajectory shaping in practical casting scenarios. Second, the repeatability evaluation was limited to forward casting with a small number of trials. In addition, the initial angular velocity waveform was restricted to a specific class of smooth profiles represented by a Gaussian function, and the statistical variability under broader casting conditions was not investigated. Extension to more general casting motions and coupled rod-line dynamics is left for future work.

Table 3. Peak-to-peak values [m] of rod tip vibration in forward cast experiments before and after trajectory shaping.

Condition	Trial 1	Trial 2	Trial 3	Average
Before shaping	1.10	1.12	1.27	1.16
After shaping	0.190	0.178	0.169	0.179

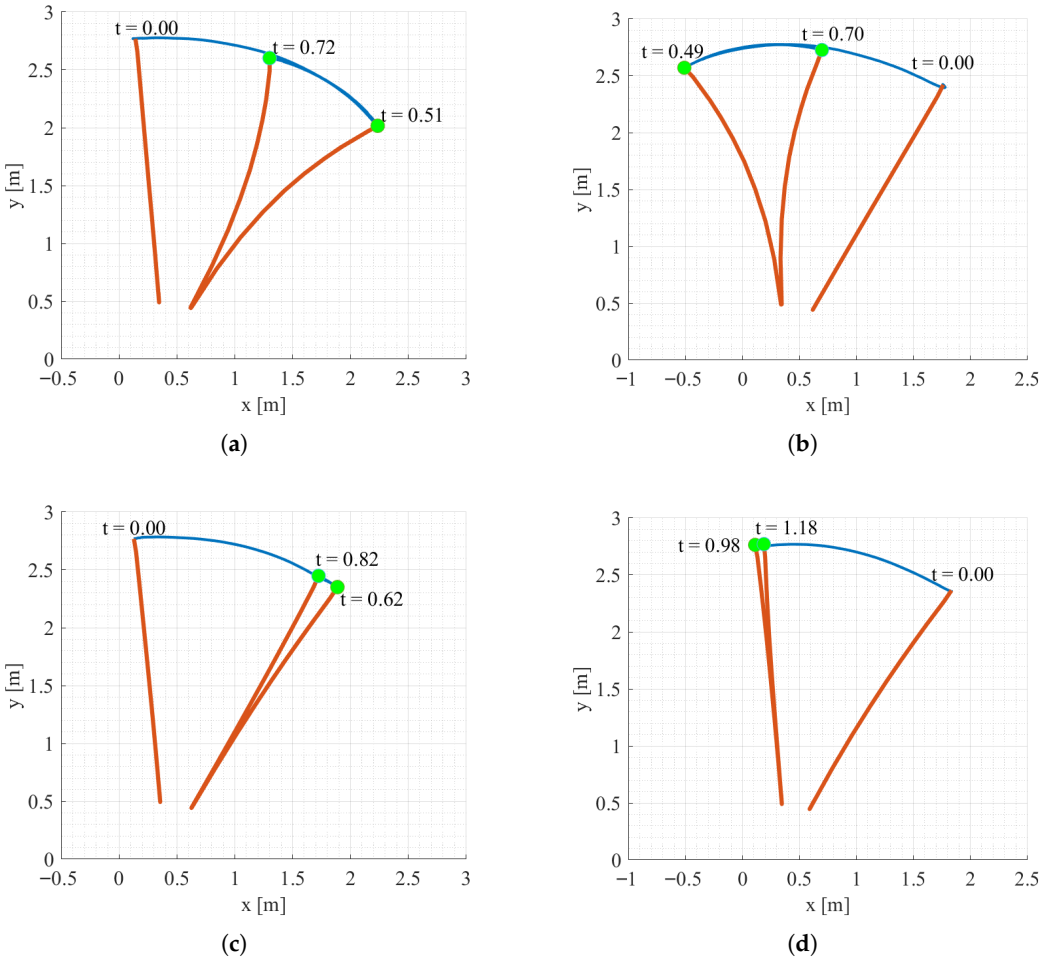
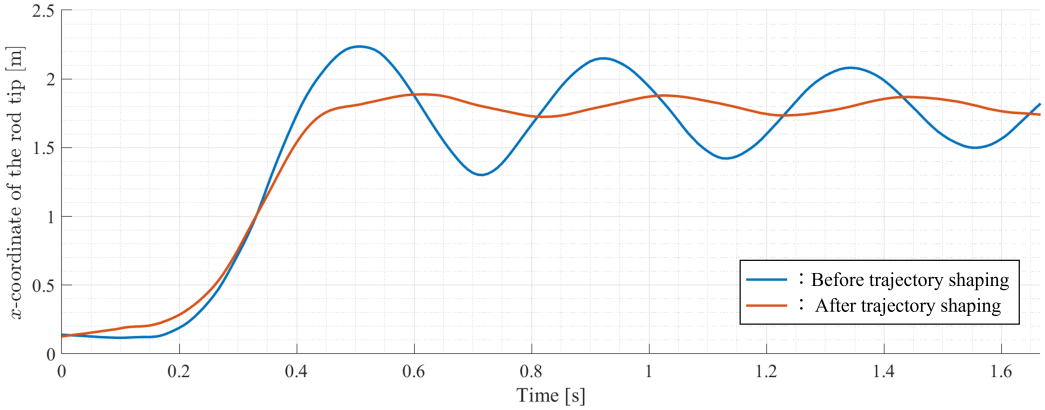
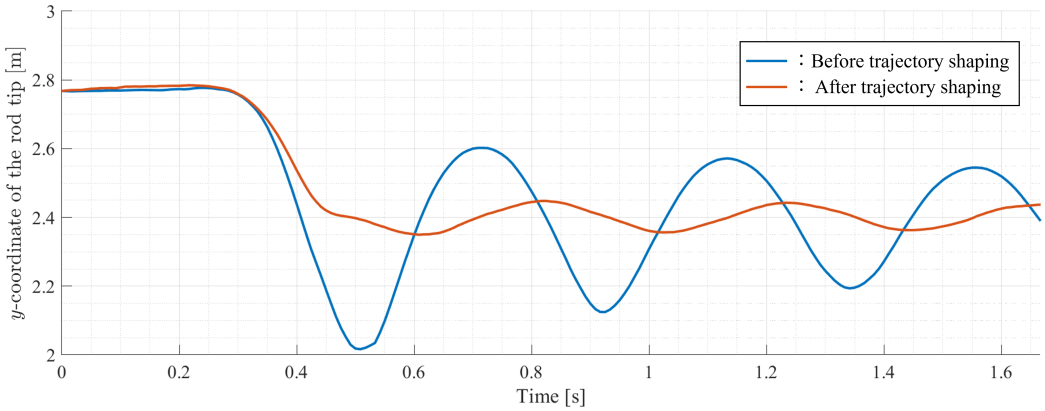


Figure 12. Comparison of rod behavior and rod tip path in each cast. The brown curve represents the rod's shape, the blue curve represents the path of the rod tip, and the green points represent the two ends of the vibration after the RSP. (**a**) Forward cast before applying the proposed method. (**b**) Back cast before applying the proposed method. (**c**) Forward cast after applying the proposed method. (**d**) Back cast after applying the proposed method.



(**a**) x-coordinate.



(**b**) y-coordinate.

Figure 13. Comparison of rod tip trajectories in forward casts. The blue line indicates the trajectory before shaping, while the brown line indicates the trajectory after shaping.

7. Conclusions

In this study, toward an engineering interpretation of the rebound phenomenon in fly-casting, we showed that the residual vibration of the rod can be suppressed by the trajectory shaping method. The main findings are summarized as follows:

- The damping of residual vibrations after the timing of the rod straight position (RSP) was defined as a vibration suppression control problem for a system with nonzero initial conditions.
- A method was proposed to estimate a second-order system model of the rod and apply a conventional trajectory shaping method to this model. Furthermore, to reduce the estimation error of the model, we applied this shaping multiple times.
- For the lifting motion, simulations demonstrated the effects of the number of trajectory shaping iterations and the parameters on the damping performance.
- It was confirmed that the waveform of the wrist angle joint obtained through trajectory shaping resembles the waveform observed in the actual rebound phenomenon, indicating the trajectory shaping method effectively reproduces the rebound phenomenon.
- Through verification using a prototype, the residual vibration of the rod tip was suppressed by the shaped trajectory. These results confirm the potential effectiveness of the trajectory shaping method for achieving motions corresponding to the rebound phenomenon.

In this study, the modeling and verification were limited to the rod system, and the dynamic effects of the line and the rod–line interaction were not considered. Future work

will address modeling and experimental verification including the line dynamics to extend the applicability of the proposed method.

In addition, although the residual vibration was significantly reduced by the proposed iterative trajectory shaping based on a second-order approximation, increasing the shaping number did not yield further damping effects, and residual vibration attributable to modeling errors remained. Future work will investigate methods to suppress this residual vibration.

Furthermore, the rebound phenomenon addressed in this study is primarily related to the formation of the rod leg. In fly-casting, however, the overall loop formation involves other elements such as the fly leg and the loop nose. The formation of these elements is expected to depend not only on the vibration suppression after the RSP but also on the design of the rod-handle trajectory before the RSP. Future studies will therefore examine the trajectory design over the entire casting motion.

Ultimately, based on the findings obtained in this study, we aim to clarify how fly-casting can be realized from an engineering perspective.

Author Contributions: Conceptualization, R.H., M.E., and Y.S.; methodology, R.H.; software, R.H.; validation, R.H.; formal analysis, R.H.; investigation, R.H.; resources, Y.S.; data curation, R.H.; writing—original draft preparation, R.H.; writing—review and editing, R.H., M.E., and Y.S.; visualization, R.H.; supervision, Y.S.; project administration, Y.S.; funding acquisition, R.H., M.E., and Y.S. All authors have read and agreed to the published version of the manuscript.

Funding: This work was partially supported by JSPS KAKENHI Grant Number JP24KJ1066 and by JKA and its promotion funds from KEIRIN RACE.

Institutional Review Board Statement: Not applicable.

Informed Consent Statement: Not applicable.

Data Availability Statement: The experimental and simulation data supporting the findings of this study are available from the corresponding author upon reasonable request. Public archiving is not provided due to the large volume of time-series data and the use of custom-built robotic hardware.

Conflicts of Interest: The authors declare no conflicts of interest.

References

1. Hakamata, R.; Endo, M.; Sugahara, Y.; Takeda, Y.; Ishii, H. Dynamic modeling and parameter identification of an elastic rod for analyzing fly-fishing. In *Proceedings of the Jc-IFToMM International Symposium*; Japanese Council of IFToMM: Tokyo, Japan, 2022; Volume 5, pp. 44–51. [CrossRef]
2. Hakamata, R.; Endo, M.; Sugahara, Y. Development of a Robot for False Casting in Fly Fishing. In Proceedings of the 2025 IEEE/ASME International Conference on Advanced Intelligent Mechatronics (AIM), Hangzhou, China, 14–18 July 2025; pp. 1–8.
3. Watanabe, T. Dynamics of a Fly Line (Double Haul Cast). *Trans. Jpn. Soc. Mech. Eng. Ser. C* **2008**, *74*, 798–805. [CrossRef]
4. Watanabe, T.; Tanaka, K. Dynamics of a Fly Line (False cast). *J. Jpn. Soc. Precis. Eng.* **2009**, *75*, 1464–1469. [CrossRef]
5. Gatti-Bono, C.; Perkins, N. Physical and numerical modelling of the dynamic behavior of a fly line. *J. Sound Vib.* **2002**, *255*, 407–414. [CrossRef]
6. Spolek, G.A. The mechanics of flycasting: The flyline. *Am. J. Phys.* **1986**, *54*, 832–836. [CrossRef]
7. Watanabe, T.; Ishida, K.; Tanaka, K. Dynamics of a Fly Line: Analysis Considering Arm Motion (Mechanical Systems). *Trans. Jpn. Soc. Mech. Eng. Ser. C* **2007**, *73*, 2531–2536. [CrossRef]
8. Kyte, A. *Orvis Guide to Better Fly Casting: A Problem-Solving Approach*; Rowman & Littlefield: Lanham, MD, USA, 2008.
9. Gammel, B.; Gammel, J. The Five Essentials of Fly Casting. In *The Loop*; Federation of Fly Fishers: Livingston, MT, USA, 2009.
10. Higashi, T. *Controlled Fly Casting Revised*; Tsuribitosha: Tokyo, Japan, 2023. (In Japanese)
11. Tetsuya, W.; Kihachiro, T. Dynamics of a Fly Line: Behavior of rebound. *J. Jpn. Soc. Precis. Eng.* **2007**, *73*, 600–604. [CrossRef]
12. Gatti-Bono, C.; Perkins, N. Comparison of numerical and analytical solutions for fly casting dynamics. *Sports Eng.* **2003**, *6*, 165–175. [CrossRef]
13. Gatti-Bono, C.; Perkins, N. Numerical model for the dynamics of a coupled fly line/fly rod system and experimental validation. *J. Sound Vib.* **2004**, *272*, 773–791. [CrossRef]

14. Watanabe, T.; Tanaka, K. Dynamics of a Fly Line (Modeling and Analysis). *Trans. Jpn. Soc. Mech. Eng. Ser. C* **2003**, *69*, 1065–1071. [CrossRef]
15. Watanabe, T.; Tomoda, A. Dynamics of a Fly Line (Roll cast). *Precis. Eng. J.* **2013**, *79*, 104–111. [CrossRef]
16. Mohamed, Z.; Tokhi, M.O. Command shaping techniques for vibration control of a flexible robot manipulator. *Mechatronics* **2004**, *14*, 69–90. [CrossRef]
17. Singhose, W. Command shaping for flexible systems: A review of the first 50 years. *Int. J. Precis. Eng. Manuf.* **2009**, *10*, 153–168. [CrossRef]
18. Newman, D.; Vaughan, J.; Hong, S. The Design of Input Shapers Which Eliminate Nonzero Initial Conditions. *J. Dyn. Syst. Meas. Control* **2018**, *140*, 101005. [CrossRef]
19. Singh, T.; Bušek, J.; Vyhlídal, T. Distributed-delay input shaper with Bernstein polynomial kernel function. *Automatica* **2024**, *166*, 111720. [CrossRef]
20. Acuity Inc. Flex 13: OptiTrack Camera Products. 2026. Available online: https://www.motioncapture.jp/optitrack/products/camera/flex13.html (accessed on 8 February 2026).

Disclaimer/Publisher's Note: The statements, opinions and data contained in all publications are solely those of the individual author(s) and contributor(s) and not of MDPI and/or the editor(s). MDPI and/or the editor(s) disclaim responsibility for any injury to people or property resulting from any ideas, methods, instructions or products referred to in the content.